Yang *et al. BMC Infectious Diseases* (2026) 26:1024
https://doi.org/10.1186/s12879-026-13234-5

BMC Infectious Diseases

RESEARCH Open Access

Plasma extracellular vesicle proteomic analysis identifies WARS as a potential biomarker of infectious mononucleosis

Li Yang[1,2], Mingjuan Jiang[1,2], Yujie Xin[1,2], Yan Xie[1,2], Pengfei Cao[1*] and Jianhong Lu[1,2*]

Abstract

Background Infectious mononucleosis (IM), caused by Epstein–Barr virus (EBV) infection, is a prevalent disease among children and young adults and may lead to a range of severe complications. Proteomic analysis of extracellular vesicles (EVs) has shown potential for identifying novel biomarkers and therapeutic targets. Consequently, elucidating the proteome signature of plasma EVs in IM may provide insights into pathological mechanisms of this disease, enabling improved diagnostic accuracy and targeted therapeutic development.

Methods In this study, we employed tandem mass tag (TMT)-labeled liquid chromatography–mass spectrometry (LC–MS) to perform differential proteomic analysis of plasma EVs between IM patients and healthy controls. Gene Ontology (GO) enrichment analysis, Kyoto Encyclopedia of Genes and Genomes (KEGG) enrichment analysis and Search Tool for the Retrieval of Interacting Genes/Proteins (STRING) database analysis were employed to conduct bioinformatics analyses. Western blotting (WB) and enzyme-linked immunosorbent assay (ELISA) were utilized to validate the differentially expressed proteins in plasma EVs. Receiver operating characteristic (ROC) curve analysis was performed to evaluate the diagnostic potential of the candidate biomarker, and Spearman correlation analysis was conducted to assess its relationship with EBV viral load.

Results We identified 193 differentially expressed proteins in plasma EVs, including 146 upregulated and 47 downregulated proteins in the IM group. Significant alterations were observed across various metabolic, immune-regulating processes, and lipid metabolism processes. Functional analysis highlighted the proteasome as a significantly enriched pathway, while also revealing differentially expressed proteins associated with crucial inflammatory and disease-related pathways, including the IL-17 signaling pathway and acute myeloid leukemia. Furthermore, we validated the upregulation of tryptophan-tRNA ligase, cytoplasmic (WARS), in clinical plasma EV samples from IM patients. The diagnostic value of EV WARS was evaluated by ROC curve analysis, which yielded an area under the curve (AUC) of 0.8091, with a sensitivity of 64.52% and a specificity of 83.33% for distinguishing IM patients from healthy controls. Additionally, EV WARS concentration in IM patients exhibited a moderate positive correlation ($r = 0.4980$, $p = 0.0044$) with EBV viral load.

*Correspondence:
Pengfei Cao
caopengfei66@163.com
Jianhong Lu
jianhlu@csu.edu.cn

Full list of author information is available at the end of the article

Conclusions Our findings provide a comprehensive plasma EV protein expression profile of IM, and indicate the potential value of WARS for IM diagnosis. This study contributes to a deeper understanding of IM pathophysiology and lays the groundwork for future diagnostic studies.

Keywords Biomarker, Extracellular vesicle, Infectious mononucleosis, Proteomics, WARS

Introduction

Epstein–Barr virus (EBV), a member of the gamma-herpesvirus subfamily, infects over 90% of the global population and is associated with various diseases, including autoimmune disorders and cancers [1]. Primary EBV infection is typically transmitted through kissing, blood transfusion, and the exchange of oral secretions [2]. While most individuals remain asymptomatic following primary EBV infection, up to 75% may develop infectious mononucleosis (IM), characterized by excessive CD8 + T-cell proliferation and an intense inflammatory response [3].

Patients with IM frequently present with sore throat, swollen cervical lymph nodes, fatigue, and physical discomfort. Additionally, approximately 20% of patients may experience abdominal pain, hepatosplenomegaly, vomiting, rash, or periorbital edema [2]. Numerous studies have shown that a history of IM significantly increases the risk of Hodgkin lymphoma (HL) and multiple sclerosis (MS) [4, 5]. Clinically, IM diagnosis relies on common symptoms and laboratory tests, including the presence of atypical lymphocytes (≥ 10%), heterophile antibodies (monospot tests), and IgM antibodies. However, these diagnostic criteria are not universally applicable. Some individuals, particularly young children, may lack typical IM symptoms or fail to produce heterophilic antibodies, potentially leading to misdiagnosis. Furthermore, EBV viral capsid antigen (VCA) IgM antibody testing may yield inaccurate results because of cross-reactivity with other pathogens [2]. Currently, neither antiviral drugs nor glucocorticoids have proven effective in reducing the severity or duration of IM [6]. Therefore, analyzing altered signaling pathways and constructing molecular interaction networks are crucial for elucidating the molecular mechanisms underlying IM, which may advance diagnostic and therapeutic strategies, as well as the exploration of IM-related complications.

Extracellular vesicles (EVs), including exosomes and ectosomes, are lipid bilayer-enclosed particles that carry diverse biological substances, such as proteins, RNA, and lipids [7, 8]. Studies indicate that EVs mediate intercellular communication, regulate signaling pathways, and modulate the progression of various diseases, positioning them as potential diagnostic or therapeutic targets [9]. Additionally, EV proteomics has emerged as a promising approach for identifying pathological features and discovering potential disease biomarkers [10, 11].

In this study, we observed notable alterations in the plasma EV proteome of patients with IM patients compared to healthy controls, and identified an upregulation of WARS in the patient cohort. Our findings may lay a groundwork for future explorations into IM pathogenesis and indicate a potential role for WARS as a biomarker.

Materials and methods

Clinical plasma sample collection

This study enrolled 58 patients diagnosed with IM, with healthy individuals recruited as the control group. All patient blood samples were collected at Xiangya Hospital, Central South University, China. The diagnosis of IM was based on clinical presentation (fever, hepatosplenomegaly and lymphoadenopathy), the heterophile antibody test, and serum EBV-DNA detection by real time-PCR. A combination of three clinical indicators and one non-specific laboratory test must be met for the diagnosis of EBV-IM. The participant information is listed in Table S1. Patients who had concurrent infections with other pathogens, or who suffered from autoimmune diseases, immunodeficiency disorders, or malignant tumors were excluded. The healthy control group consisted of volunteers without any clinical symptoms. These samples were drawn into heparin anticoagulant tubes and subsequently centrifuged at 4000 rpm for 5 min to isolate plasma.

EV isolation

Plasma samples obtained from patients diagnosed with infectious mononucleosis (IM) and healthy control subjects were initially subjected to the depletion of high-abundance proteins, specifically albumin and immunoglobulin G (IgG), using a commercial kit (Sigma–Aldrich, St. Louis, MO, USA). Subsequently, EVs were isolated from the processed plasma samples using the ExoQuick™ kit (System Biosciences Inc, Mountain view, CA). Briefly, the EV precipitation solution was added to the treated plasma sample at a volumetric ratio of 1:4, and then the mixture was refrigerated at 4 °C overnight. After the mixture was centrifuged at 1500 × g for 30 min in next day, the EV pellets were resuspended in nuclease-free water.

Transmission electron microscopy (TEM) assay

EV samples were deposited onto Formvar-carbon-coated grids, and subsequently fixed with 4% paraformaldehyde, and then were stained with uranyl acetate. The samples

were visualized with an FEI Tecnai12 transmission electron microscope.

Fluorescence in situ hybridization (FISH)

As described in the previous study, an EBV-specific probe was employed to identify the EBV genome within peripheral blood mononuclear cells (PBMCs) in IM [12]. Briefly, PBMCs were smeared onto slides, followed by immersion, denaturation, and dehydration processes. Subsequently, the slides were incubated with a hybridization mixture containing 50 ng of the probe and 5 μg of salmon sperm DNA. This was followed by incubation with an anti-FITC antibody. After multiple washing and drying steps, the slides were analyzed using fluorescence microscope.

Protein quantification and Coomassie Brilliant Blue staining

The EV protein concentration was measured

with a bicinchoninic acid (BCA) protein assay kit (Vazyme, China). After the EV proteins were separated by SDS-PAGE for protein visualization, the gel was stained using a Coomassie Brilliant Blue R-250 solution or G-250 solution for 1 h at room temperature. Subsequently, the gel was destained in a solution containing 25% Ethanol and 2% glacial acetic acid until the protein bands were clearly visible against a transparent background.

Peptide preparation

We selected 6 samples of plasma EVs from patients with infectious mononucleosis and 6 samples from healthy controls for TMT-labeled LC-MS/MS proteomics analysis. After protein extraction from the EV samples, dithiothreitol (DTT) was added to the samples to a final concentration of 2 mM, followed by the addition of sufficient iodoacetic acid. Proteins were precipitated by adding 4 volumes of prechilled acetone, and the precipitate was collected by centrifugation. The precipitate was finally dissolved in a lysis buffer containing 0.1 M triethylammonium bicarbonate (TEAB, pH 8.5) and 8 M urea. The protein samples were digested with Trypsin Gold (Promega). The peptides were desalted using C18 cartridges to remove high concentration of urea, and the desalted peptides were subsequently dried using vacuum centrifugation.

TMT labeling of peptides

Desalted peptides were labeled with TMT reagents, following the manufacturer's instructions. For labeling, 1 unit of TMT reagent was added per 0.1 mg of peptides. After incubation, the reaction was stopped with ammonium hydroxide. Differentially labeled peptides were mixed equally and then desalted using peptide desalting spin columns (ThermoFisher, 89852).

HPLC fractionation

The TMT-labeled peptide mixture was fractionated on a Rigol L3000 HPLC system equipped with a Waters BEH C18 column (4.6 × 250 mm, 5 μm) at a flow rate of 1 mL/min. The column temperature was maintained at 50 °C. A binary mobile phase system consisting of phase A (2% acetonitrile, pH adjusted to 10.0 with ammonium hydroxide) and phase B (98% acetonitrile, pH adjusted to 10.0 with ammonium hydroxide) was employed for gradient elution. The tryptic peptides were monitored at 214 nm UV wavelength. Eluates were collected at 1-minute intervals and subsequently pooled into 15 fractions. The collected fractions were dried under vacuum and redissolved in a 0.1% (v/v) formic acid aqueous solution for downstream analytical procedures.

LC-MS/MS analysis

Shotgun proteomics analyses were performed using an EASY-nLC™ 1200 UHPLC system (ThermoFisher) coupled to an Orbitrap Q Exactive HF-X mass spectrometer (ThermoFisher) in data-dependent acquisition (DDA) mode. The peptide concentration of each fraction was determined by measuring absorbance at 280 nm with a NanoDrop8000. Subsequently, 2 μg of peptides from each fraction, reconstituted in 0.1% formic acid, was loaded onto an Acclaim PepMap100 C18 Nano-Trap column (2 cm × 100 μm, 5 μm). Peptide separation was performed on a Reprosil-Pur 120 C18-AQ analytical column (15 cm × 150 μm, 1.9 μm) with a 90-minute linear gradient for TMT6-plex labeling. The gradient progressed from 5% to 100% mobile phase B (0.1% FA in 80% acetonitrile) in mobile phase A (0.1% FA in water) at a flow rate of 600 nL/min. For DDA, the Q-Exactive HF-X mass spectrometer was operated in positive polarity mode. Full-scan mass spectra were acquired in the range of 350–1500 m/z, and a maximum number of 40 of the most abundant precursor ions were selected for higher energy collisional dissociation (HCD) fragment analysis.

Deposition of proteomic data

The mass spectrometry proteomics data have been deposited to the ProteomeXchange Consortium (http://proteomecentral.proteomexchange.org) via the iProX partner repository [13] with the dataset identifier PXD025952.

Data processing and protein identification

The raw mass spectrometry data were retrieved using the Proteome Discoverer 2.2 software. Protein identification and quantification were conducted by searching the data against the human UniProt database (version homo_sapiens_uniprot_2018.06). To improve the quality of the analytical results and reduce false positives, the software implemented additional filtration criteria for the search

results, and retained only peptides and proteins with a false discovery rate (FDR) below 5%.

Bioinformatic and functional enrichment analysis

Gene Ontology (GO) and Kyoto Encyclopedia of Genes and Genomes (KEGG) pathway enrichment analyses were performed to investigate the biological significance of the differentially expressed proteins. The analysis was based on a hypergeometric test. Given the limited number of differentially expressed proteins identified in this proteomic analysis, a standard False Discovery Rate (FDR) correction only yielded a few significantly enriched terms. Therefore, to facilitate the generation of biological hypotheses, we reported the results based on a less stringent criterion. GO terms and KEGG pathways with a p-value ≤ 0.05 were considered significantly enriched. For the protein-protein interaction (PPI) network analysis, differentially expressed proteins were submitted to the Search Tool for the Retrieval of Interacting Genes/Proteins (STRING) database, and the network was constructed using a minimum required interaction score (confidence) of 0.5 and subsequently visualized using Cytoscape software.

Western blot (WB)

After the EV protein concentration was measured using a BCA protein assay kit, equal amounts of total EV protein were initially separated by SDS–PAGE and subsequently transferred onto a polyvinylidene fluoride (PVDF) membrane. The membrane was blocked with 5% (w/v) nonfat milk for 1 h at room temperature, followed by an overnight incubation with the relevant primary antibody at 4 °C. After three washes, the membrane was incubated with the secondary antibody for 1 h at 37 °C. The protein bands were visualized using an enhanced chemiluminescene (ECL) detection system. The antibodies used in this study are listed in Table S2.

Enzyme-linked immunosorbent assay (ELISA)

The concentration of WARS in plasma-derived EVs was quantified using a commercial ELISA kit (Jianglai Bio, Shanghai, China) according to the manufacturer's instructions. Briefly, EVs were extracted from equivalent volumes of plasma and resuspended in equal volumes, Subsequently, an equal volume of the EV suspension from each sample was added to a pre-coated microplate. Following incubation and washing steps, the optical density (OD) was subsequently measured at 450 nm. Sample WARS concentrations were calculated by interpolation from a standard curve generated using known concentrations of recombinant WARS protein.

Statistical analysis

The grayscale intensity of Western blot bands was quantified using ImageJ software. As the experiment involved a large number of samples, blotting was performed across multiple membranes. To correct for inter-membrane variability, a two-step normalization was applied: WARS protein intensity was first normalized to total protein (Coomassie staining), then standardized to the average of healthy controls on each membrane. Normalized values were pooled across membranes for statistical comparison. Statistical analyses were performed with GraphPad Prism version 8.0.1. Intergroup comparisons were conducted using a two-tailed Student's t tests. Receiver Operating Characteristic (ROC) curve analysis was performed to evaluate the potential predictive value of EV-WARS protein for IM, and the Area Under the Curve (AUC) with its 95% confidence interval (CI) was calculated. The optimal diagnostic cut-off was determined by identifying the point on the ROC curve closest to the top-left corner (0,1), which minimizes the euclidean distance calculated as $[(1\text{-sensitivity})^2 + (1\text{-specificity})^2]$ [14, 15]. The correlation between plasma EBV copy numbers and EV-WARS levels was evaluated using Spearman correlation analysis. A P-value < 0.05 was considered statistically significant.

Results

Biological characterization of plasma EVs

To determine whether the isolated components were EVs, TEM and WB were employed to identify their characteristics. Under TEM, the EV exhibited a typical 'cup-shaped' morphology (Fig. 1A). Furthermore, we employed the WB method to examine the expression and purity of EV markers. In this analysis, total cell lysate (Cell) was used as a positive control to validate the efficacy of the antibodies for all target proteins and to confirm the molecular size of each marker. The results showed that, compared to the original plasma (Plasma), the positive EV markers heatshockprotein70 (HSP70) and CD9 were expressed at higher levels in our isolated EVs, indicating effective enrichment of EVs. Another positive marker, tumor susceptibility 101 (TSG101), was also expressed in the EV sample. As a critical assessment of purity, the non-EV endoplasmic reticulum protein, Calnexin, was clearly visible in the cell lysate control and was also detected in the raw plasma, but was nearly undetectable in our final EV sample. This series of results showed that we successfully isolated and purified EVs from plasma (Fig. 1B, Fig. S1). We also used Coomassie Brilliant Blue staining for each group of samples to determine the total amount of protein loaded onto each sample (Fig. S2). FISH analysis of PBMCs from IM patients demonstrated intracellular punctate fluorescence, confirming the presence of the EBV genome (Fig. 1C).

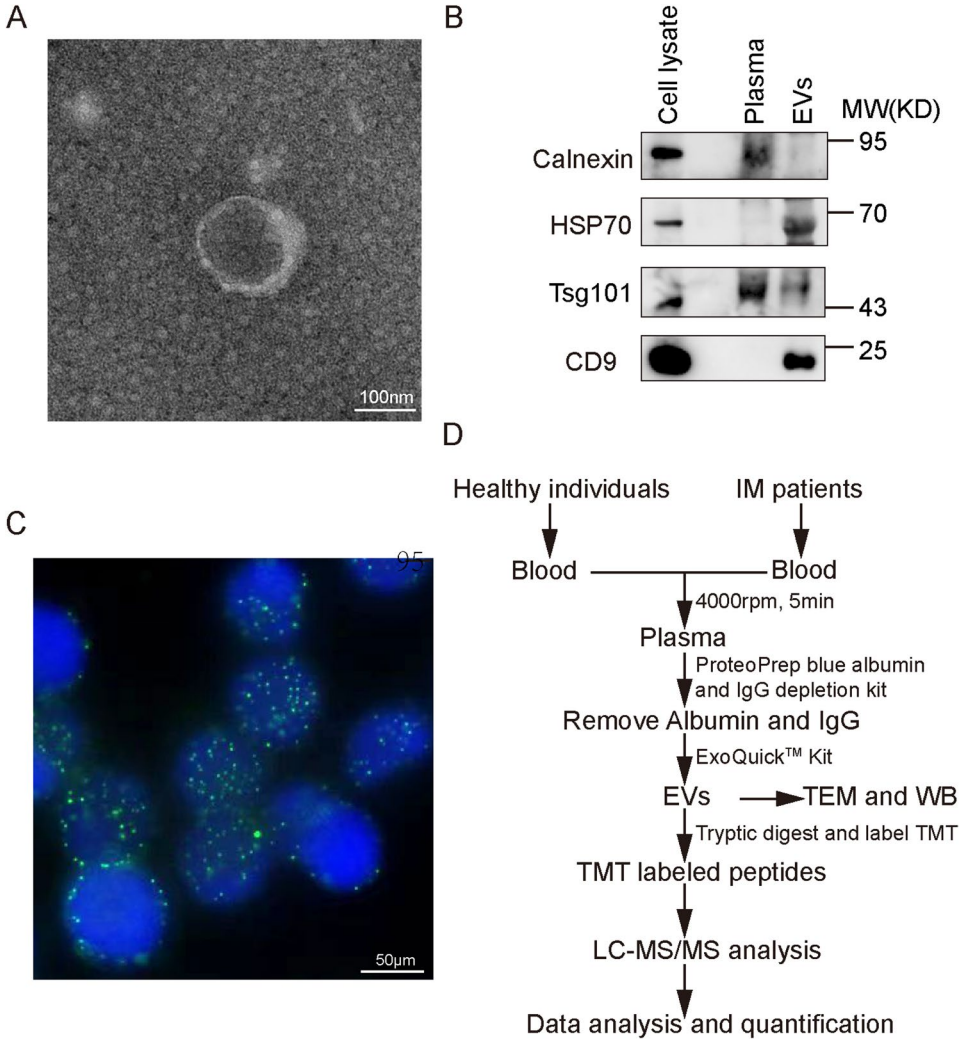

Fig. 1 Characterization of EVs and the EBV genome. (**A**) Representative transmission electron micrograph (TEM) showing the cup-shaped morphology of the EVs. (**B**) Identification of EV markers. Western blot analysis was performed on a set of samples, including total cell lysate, plasma, and the corresponding purified EVs derived from the plasma sample. The blot was probed for EV-positive markers (HSP70, TSG101, and CD9) and the EV-negative marker, calnexin. (**C**) FISH assay for detecting the EBV genome in PBMCs from IM patients. (**D**) Schematic of the workflow for EV isolation and subsequent proteomic analysis

Plasma EVs from healthy individuals and IM patients were isolated, purified, and analyzed by TMT-labeled quantitative proteomics to investigate differential protein profiles (Fig. 1D).

Differential protein analysis of plasma EV proteomics

To ensure the reliability of the mass spectrometry data, we evaluated the peptide length distribution and protein molecular weight range. The analysis revealed that the identified peptides spanned from 7 to 25 amino acid residues, confirming the efficacy of proteolysis (Fig. 2A). Furthermore, the protein molecular weight distribution exhibited a broad spectrum, indicating comprehensive protein coverage (Fig. 2B). Additionally, the precursor ion tolerance was predominantly centered around 0, suggesting a small mass deviation (Fig. 2C). After a search against the protein database (UniProt), 913 proteins were identified in both groups. In order to comprehensively construct the differential protein expression profile of IM and maximize the discovery of potential biomarkers, proteins with a $|\text{fold change}| \geq 1.2$ and a p-value < 0.05 were considered significantly differentially expressed. Statistical analysis identified 193 significantly differentially expressed proteins, including 146 upregulated and 47 downregulated proteins in the IM group (Fig. 2D, Table S3). The differential protein profile was further visualized through hierarchical clustering analysis and a volcano plot (Fig. 2E and F). Following the exclusion of proteins lacking gene annotations, we categorized and ranked the top 10 most significantly upregulated and downregulated proteins (Table 1).

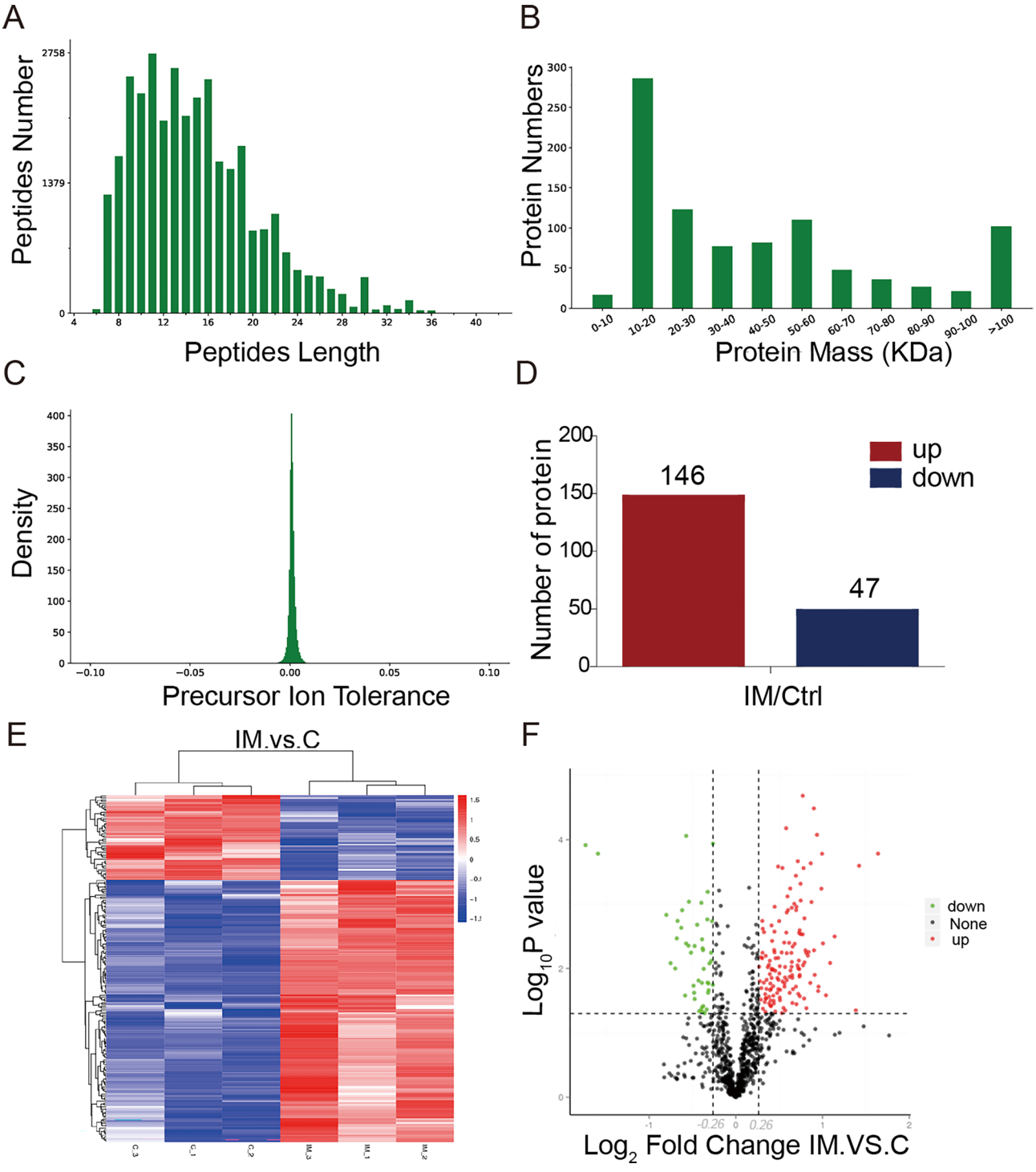

Fig. 2 Differential protein analysis of the plasma EV proteome. (**A**-**C**) Quality control and analysis of the proteomic data. (**D**) Comparative quantification of differentially expressed proteins between IM patients and healthy controls. (**E**) Heatmap depicting hierarchical clustering of upregulated and downregulated protein expression profiles in IM. (**F**) Volcano plot showing the statistical significance of differentially expressed proteins between IM patients and healthy controls

Bioinformatics analyses of differentially expressed proteins

To elucidate the functional implications of the differentially expressed proteins, comprehensive bioinformatics analyses were conducted, including GO annotation, KEGG pathway enrichment, and protein–protein interaction network construction (Fig. 3). The GO biological process analysis demonstrated significant enrichment in metabolic and catabolic regulation, particularly in

Table 1 The top 10 upregulated or downregulated proteins

Number	Gene	Description	IM.vs. C UP/DOWN	IM.vs. C FC	IM.vs. C Pvalue
1	CRP	C-reactive protein	up	3.5742	0.0000
2	WARS	Tryptophanyl-tRNA synthetase, cytoplasmic	up	2.6786	0.0003
3	PSM8	Proteasome subunit beta type	up	2.6100	0.0446
4	HEL-S-275	Proteasome endopeptidase complex	up	2.2024	0.0032
5	S100A8	Protein S100-A8	up	2.1252	0.0082
6	SAA1	Serum amyloid A-1 protein	up	2.0066	0.0041
7	SAA2	Serum amyloid A-2 protein	up	1.9925	0.0002
8	PSMB10	Proteasome subunit beta type-10	up	1.9365	0.0191
9	DCXR	L-xylulose reductase	up	1.9306	0.0223
10	LCP1	Plastin-2	up	1.9125	0.0001
11	KRT85	Keratin, type II cuticular Hb5	down	0.3007	0.0001
12	SERPINA1	Alpha-1-antitrypsin	down	0.3320	0.0002
13	FN1	Fibronectin 1, isoform CRA_n	down	0.5933	0.0083
14	RSU1	RSU1 protein (Fragment)	down	0.6160	0.0100
15	HEL-S-51	Epididymis secretory protein Li 51	down	0.6236	0.0034
16	TUBB1	Tubulin beta-1 chain	down	0.6276	0.0018
17	APOL1	Apolipoprotein L, 1, isoform CRA_b	down	0.6464	0.0023
18	THBS1	Thrombospondin 1, isoform CRA_a	down	0.6508	0.0012
19	PARVB	Beta-parvin	down	0.6666	0.0263
20	IGLV4-3	Immunoglobulin lambda variable 4 – 3	down	0.6721	0.0041

"metabolic process", "organic substance metabolic process", "macromolecular metabolic process", and "proteolysis involved in cellular protein catabolic process". Notably, immune-related processes, such as "innate immune response" and "inflammatory response", also exhibited obvious alterations (Fig. 3A). The proteasome was the only pathway identified as significantly enriched by the KEGG analysis. In addition, enrichment trends were noted in various metabolic pathways, the IL-17 and TNF signaling pathways, although these did not reach statistical significance (Fig. 3B). The top twenty enriched biological processes and pathways are listed in Tables S4 and S5, respectively. Protein-protein interaction networks were constructed using STRING database and subsequently visualized through Cytoscape, which identified key hub proteins (Fig. 3C and D). Among the upregulated proteins, C-reactive protein (CRP); L-lactate dehydrogenase A chain (LDHA); myeloperoxidase (MPO); L-lactate dehydrogenase B chain (LDHB); catalase (CAT); and transaldolase (TALDO1) exhibited extensive connectivity (Fig. 3C). Moreover, apolipoprotein A-I (APOA1), fibronectin 1 (FN1), and serum albumin (ALB) emerged as central nodes within the downregulated protein network (Fig. 3D). These findings suggest that these molecules may play pivotal roles in the pathogenesis of IM.

Validation of WARS upregulation in plasma EVs and the assessment of its diagnostic performance

As shown in Table 1, WARS exhibited the second highest upregulation level among all detected gene, surpassed only by the well-characterized acute phase reactant CRP, a canonical biomarker of inflammatory responses. Therefore, we focused on WARS to validate the proteomic findings. Initial validation was performed using plasma EV samples from the proteomics cohort, and Western blot analysis confirmed that WARS expression was consistent with the proteomics data (Fig. 4A and B). The total protein loading amount in each sample was determined by Coomassie blue staining (Fig. 4C and D). To strengthen the evidence, we expanded the validation to include additional plasma EV samples from both IM patients and healthy controls, which further demonstrated elevated WARS expression in the IM cohort (Fig. S3).

Quantitative analysis of the Western blots revealed that the expression level of the WARS protein was significantly upregulated in IM patients compared to the healthy control group (Fig. 5A). To ensure accurate quantification, the signal intensity of the protein bands was normalized to the total protein amount in each lane, as determined by Coomassie Brilliant Blue staining. We also collected additional patient samples for further validation. The increased protein levels of WARS in the plasma EVs of IM patients, previously observed in proteomic and Western blot analyses, were further confirmed by quantitative ELISA (Fig. 5B). To evaluate the diagnostic performance of WARS in differentiating IM patients from healthy controls, a ROC curve analysis was performed on the WARS ELISA results (Fig. 5C). The analysis yielded an area under the curve (AUC) of 0.809 (95% CI: 0.691–0.927, $p = 0.0003$), suggesting its potential as a diagnostic biomarker. Using theYouden's J statistic (closest-to-(0,1) corner method), an optimal cut-off value of 0.1827ng/

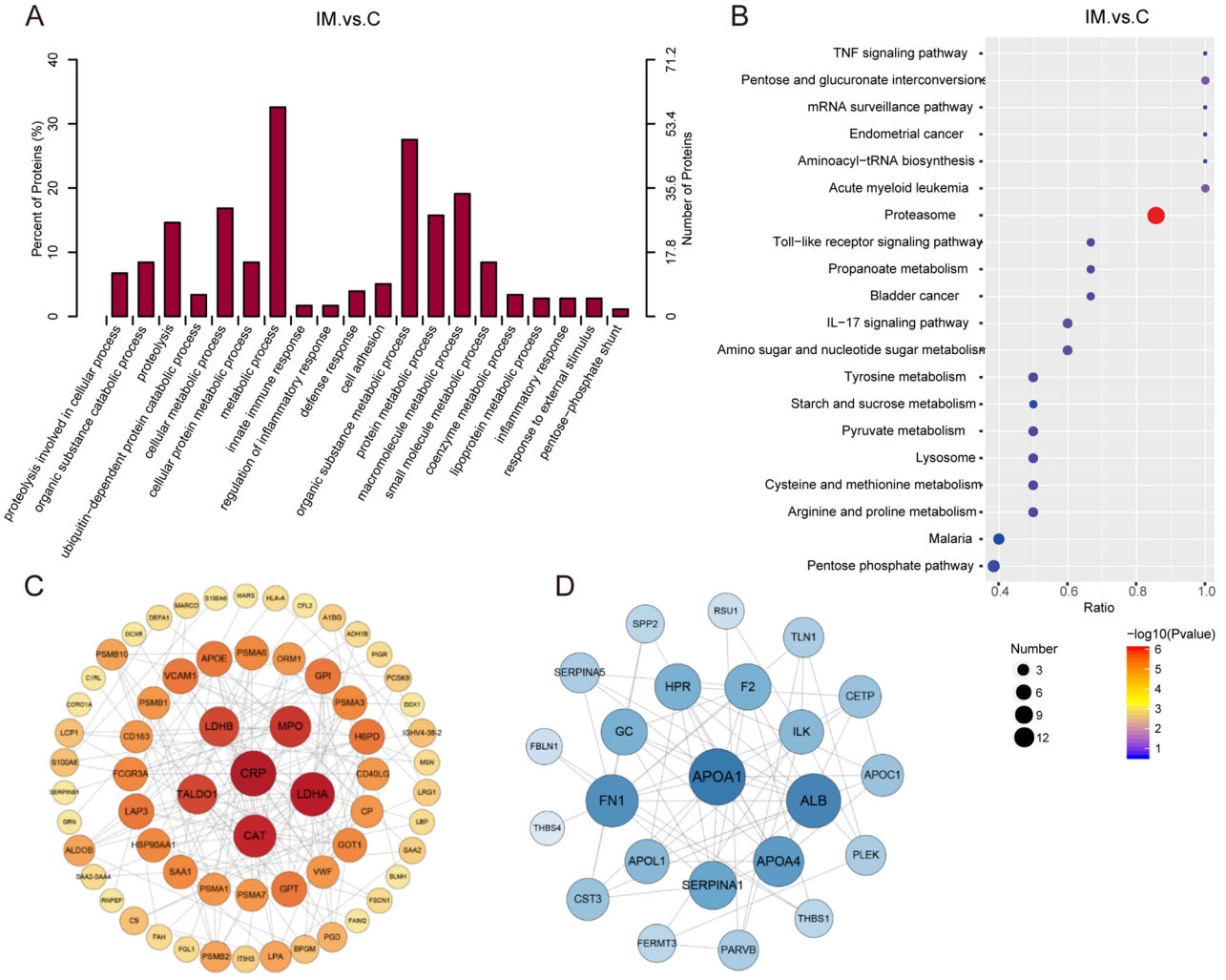

Fig. 3 Bioinformatics analyses of differentially expressed proteins. (**A**) Gene Ontology (GO) enrichment analysis of biological process (BP) terms associated with the differentially expressed proteins. (**B**) KEGG pathway analysis identifying significantly enriched pathways. (**C**) Protein–protein interaction (PPI) network of upregulated proteins in IM patients. (**D**) PPI network of downregulated proteins in IM patients

mL was established, which corresponded to a sensitivity of 64.52% and a specificity of 83.33%. Furthermore, to determine if WARS levels in plasma EVs are associated with EBV infection, we performed a correlation analysis based on the ELISA data. As illustrated in the scatter plot (Fig. S4), there was a moderate but statistically significant positive correlation between the WARS concentration and the EBV viral load ($r = 0.4980$, $p = 0.0044$). Which indicates that EBV viral load influences WARS protein levels to some extent.

Discussion

Recently, Kazunori Haruta et al. reported the plasma protein profile of patients with IM [16]. Consistent with their analysis of the total plasma proteome, our proteome data of plasma EVs in IM also revealed a significant upregulation of multiple proteins associated with immune activation and inflammatory responses, such as lectin galactoside-binding soluble 3 binding protein (LGALS3BP), leucine-rich alpha-2-glycoprotein 1 (LRG1), and LDHB. Furthermore, our pathway analysis similarly showed an enrichment of related biological processes, including the 'inflammatory response'. These converging findings confirm that both total plasma and EV proteomics effectively capture a core pathological feature of IM: a state of elevated host immune and inflammatory activation.

Notably, the plasma proteomics study of IM patients by Haruta et al. primarily revealed the activation of systemic immune processes, such as the complement system, positive regulation of cytokine production. In our study, while our EV proteomics analysis also detected the enrichment of immune processes, a far more dominant biological signature pointed towards protein degradation pathways. This was underscored by both GO functional analysis, which highlighted protein catabolic processes,

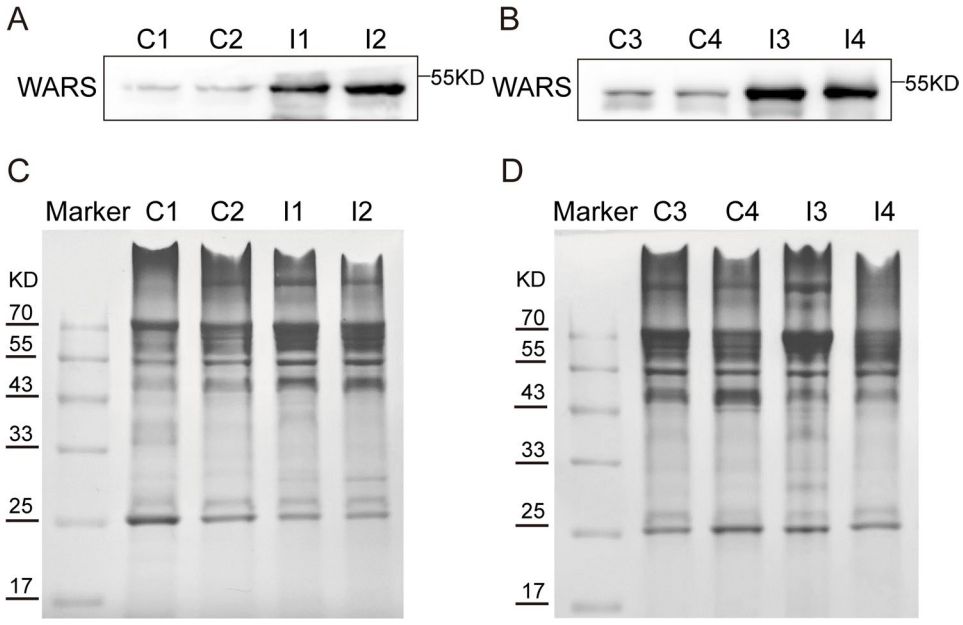

Fig. 4 Validation of proteomic analysis through WARS protein expression in plasma EVs. (**A**) Western blot analysis of WARS protein in EV samples used for TMT proteomics (C: healthy control; I: IM patient). (**B**) Comparison of WARS protein expression in EV samples between healthy controls and IM patients. (**C**-**D**) Coomassie Brilliant Blue staining to determine total protein loading across samples

and KEGG pathway analysis, which identified the proteasome pathway as the most significantly enriched. Consistent with this, a significant enrichment of proteasome subunits (e.g., proteasome subunit beta type (PMS8), proteasome subunit beta type-10 (PSMB10), proteasome subunit alpha type-3 (PSMA3), proteasome subunit alpha type (PSMA6), proteasome subunit beta type-2 (PSMB2)) within EVs was identified in our plasma EV proteome.

The proteasome is a key line of defense for the host cell, responsible for degrading viral proteins and resisting viral replication [17, 18]. It has been demonstrated that proteasomes can be packaged as active proteases into EVs for release, serving as a medium for intercellular communication in response to pathogen invasion or severe proteotoxic stress [19, 20]. During a viral infection, the massive synthesis of viral proteins within an infected cell may exceed its individual processing capacity. Therefore, our observation of proteasome enrichment in EVs from IM patients may unveil a sophisticated host defense strategy, wherein cells purposefully package certain proteasome subunits into EVs for extracellular release to help infected cells degrade viral proteins to maintain cellular proteostasis. This reveals a strategy by which cells utilize intercellular communication to resist viral infection and replication.

Beyond the proteasome, our study identified WARS as a key protein highly enriched in EVs but undetectable in the total plasma proteome. During bacterial infections, activated monocytes release WARS, which then engages toll-like receptor 2 (TLR2) and TLR4/MD-2 on macrophages to induce cytokine production and neutrophil infiltration [21]. Similarly, in response to viral infections, WARS is rapidly secreted and functions as an antiviral cytokine, promoting the production of inflammatory cytokines and type I interferons to inhibit viral replication [22]. Unlike broad acute-phase reactants like CRP and serum amyloid A protein (SAA), WARS also acts as a potent alarmin that directly reflects the activation state of the immune system, particularly the T-cell compartment [23]. There WARS may act as a functional indicator of this core pathogenic process, rather than just its downstream inflammatory consequence.

Emerging studies suggest that IM severity may also be linked to cross-reactive influenza CD8 + T-cell receptor repertoires or expansion of HLA-DR+ CD8 + T cells [24, 25]. Nuray Aslan et al. developed a severity scoring system to assess the role of cross-reactive CD8 + T cells in IM progression, categorizing patients into mild and severe groups [24]. Given that WARS has been shown to positively regulate the survival and activation of CD8 + T cells [23]. In addition, in certain diseases with extremely high inflammatory responses, such as sepsis and coronavirus disease 2019 (COVID-19), high levels of WARS are also positively correlated with the severity of the disease [26, 27]. Therefore, we hypothesize WARS levels may also positively correlate with disease severity of IM. The elevated WARS in IM not as a specific biomarker for the disease, but may as a key driver of the hyperinflammatory symptoms. Crucially, therapeutic intervention with an antibody against secreted WARS was shown to attenuate cytokine storm and organ failure in

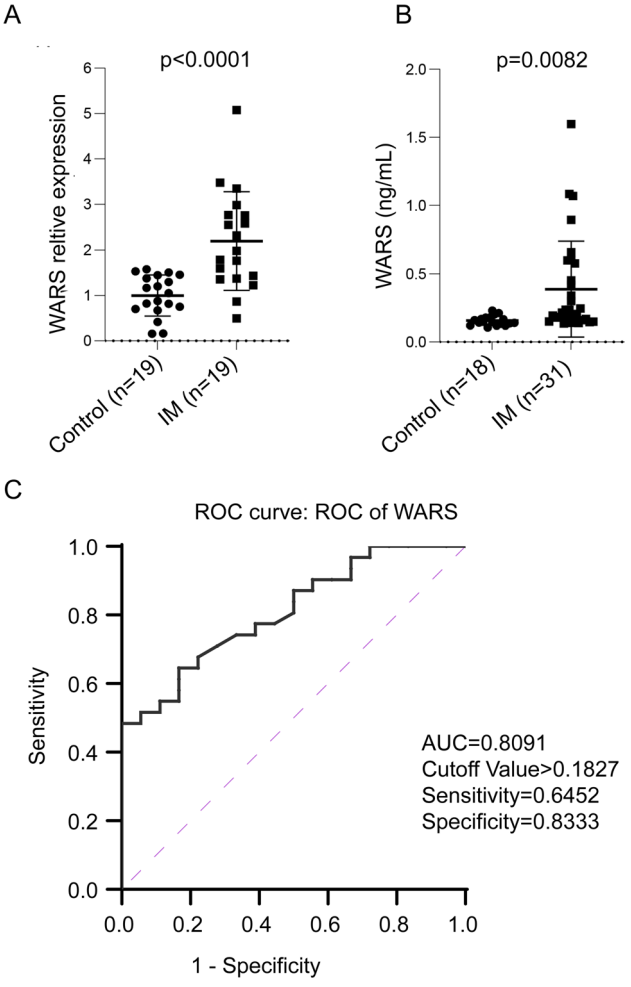

Fig. 5 Quantitative comparison of WARS protein expression in plasma EVs between healthy controls and IM patients and the assessment of its diagnostic performance. (**A**) Statistical analysis of WARS Western blot band intensity in healthy controls versus IM patients. The relative expression level of WARS was calculated by first normalizing the band intensity to the total protein load, as determined by Coomassie Brilliant Blue staining, and then comparing this value to the average of the healthy control group. (**B**) ELISA quantification of WARS protein concentration in the plasma EVs of healthy controls and IM patients. (**C**) The receiver operating characteristic (ROC) curve analysis of WARS protein for diagnosing IM. The vertical axis represents sensitivity (true positive rate), while the horizontal axis represents 1 - specificity (false positive rate). The Area Under the Curve (AUC) was calculated to quantify performance. The optimal cutoff value was determined using the closest-to-(0,1) corner method on the ROC curve, and the corresponding sensitivity and specificity are labeled

preclinical sepsis models [28]. This suggests that, antagonizing WARS could represent a novel therapeutic strategy to mitigate immune-mediated pathology. Therefore, integrating WARS protein expression with CD8 + T-cell counts may help increase the precision of IM diagnosis and treatment.

A key observation from the ELISA results is the notable heterogeneity in WARS expression levels among patients with IM. Based on this cutoff derived from the ROC curve analysis, we stratified the IM cohort into a subgroup with WARS levels comparable to healthy controls (35%, hereafter "WARS-low") and another with significantly elevated levels (65%, hereafter "WARS-high"). We posit that this bimodal expression pattern is not merely a result of random data fluctuation but rather reflects the intrinsic complexity and inter-patient variability inherent to IM. Given the correlation of high WARS levels with disease severity in other hyperinflammatory conditions like sepsis and COVID-19, we hypothesize this heterogeneity reflects variations in individual immune responses. Future studies should aim to collect comprehensive clinical information to fully elucidate the mechanisms driving the heterogeneous expression of WARS in IM patients.

In addition to WARS, our study also reveals significant alterations in the expression of other proteins in IM. Among the significantly upregulated proteins, the marked elevation of multiple interferon-stimulated genes products, such as PSMB8, and PSMB10, proteasome subunit alpha type-1 (HEL-S-275), collectively indicates a highly activated immune state. PSMB8 and PSMB10, as key components of the immunoproteasome, enhance CD8 + T cell responses through efficient processing of antigenic peptides [29], which provides a molecular explanation for the massive T-cell proliferation characteristic of IM. However, this intense immune activation is inevitably accompanied by severe systemic inflammation. Notable, preclinical studies have shown that the use of ONX 0914, a specific inhibitor of PSMB8, can suppress the resulting adverse inflammatory tissue damage [30]. Our mass spectrometry data also showed the significant upregulation of classic acute-phase proteins CRP, SAA1, SAA2, and the early danger signal protein S100-A8 (S100A8), which is likely the direct cause of clinical symptoms such as fever and fatigue in patients [31, 32]. In stark contrast to this hyperactivated immune state, the significant downregulation of several key structural proteins suggests that tissue homeostasis may be compromised. For instance, the downregulation of fibronectin 1 (FN1) and beta-parvin (PARVB), molecules crucial for maintaining extracellular matrix integrity and cell adhesion, indicates that the potent inflammatory environment may severely disrupt the structural foundation of tissues [33–35]. Furthermore, it has been established that serpin A11 (SERPINA1) deficiency is associated with chronic liver diseases [36], which may offer a potential explanation for the liver dysfunction observed in some IM patients [2, 3]. Therefore, further validation of additional molecular markers is essential to develop a more sensitive and specific multimolecular diagnostic and therapeutic approach for IM.

Several limitations of our study should be acknowledged. First, during the EV preparation process, despite minimizing plasma protein interference via a depletion

kit and confirming EV enrichment through TEM and WB, precipitation-based isolation cannot completely preclude trace non-vesicular protein co-precipitation, which should be carefully taken into account in future similar studies. Additionally, while our study primarily focused on specific protein levels, exploring potential alterations in the number and size distribution of vesicles under IM conditions remains a highly meaningful future direction. Second, the self-limiting nature of IM prevented remission-phase sample collection. This restricted a comprehensive analysis of the dynamic changes in WARS levels throughout the entire course of the disease. Third, the absence of detailed clinical data, such as patient severity scores and symptom duration, limited our ability to correlate WARS levels with disease severity. Future research should prioritize the prospective collection of these variables to better define the role of WARS as a potential prognostic or diagnostic biomarker. Furthermore, although we validated our findings using WB and ELISA in an external cohort that was independent of the initial proteomics cohort, the sample size was insufficient for robust confirmation. Future validation in a larger-scale cohort is imperative. Crucially, such a cohort should include not only well-characterized IM patients and healthy controls but also patients with other diseases presenting similar clinical symptoms to determine the specificity of WARS as a biomarker. Finally, while elevated WARS may be involved in immune regulation, its precise mechanistic role in the pathogenesis of IM remains to be elucidated. Further functional studies are required to clarify its biological mechanisms and ultimate clinical relevance.

Conclusion

This study elucidates the distinct molecular profiles of plasma EVs associated with IM, providing a foundation for further research into its pathogenesis and the development of targeted diagnostic tools. Notably, WARS upregulation in IM patients' plasma EVs was validated, suggesting its potential as a diagnostic biomarker. However, clinical applicability requires larger-scale validation to assess accuracy and its impact on clinical outcomes.

Supplementary Information

The online version contains supplementary material available at https://doi.org/10.1186/s12879-026-13234-5.

Supplementary Material 1

Supplementary Material 2

Supplementary Material 3

Supplementary Material 4

Supplementary Material 5

Supplementary Material 6

Supplementary Material 7

Acknowledgements

We thank Novogene Biotechnology, Beijing, for providing the services of TMT quantitative proteomics.

Author contributions

L.Y. was responsible for the literature search, experimental studies, data acquisition and analysis, statistical analysis, and manuscript writing. M.J., Y.X. and J.Y.X. were responsible for editing the images and tables, data analysis and result interpretation. P.C. and J.L. were responsible for the study concept and design, supervised and guided the overall research and revised the manuscript. J.L. provided experimental facilities and resources for this study. All the authors read and approved the final manuscript.

Funding

This work was supported by National Natural Science Foundation of China (82272981, 32470171) and Graduate Research and Innovation Projects of Central South University (2021zzts0320).

Data availability

The datasets used and/or analyzed during the current study are available from the corresponding author upon reasonable request.

Declarations

Ethical approval

This study was approved by the Medical Ethics Committee of Central South University (2019030160) and informed consent to participate in this study was provided by participate or the participants' legal guardian/next of kin. All experiments were performed in accordance with relevant named guidelines and regulations.

Competing interests

The authors declare no competing interests.

Author details

[1]Department of Hematology, National Clinical Research Center for Geriatric Disorders, Xiangya Hospital, Central South University, Changsha, Hunan, China
[2]Department of Microbiology, Xiangya School of Basic Medical Sciences, Central South University, Changsha, Hunan, China

Received: 2 April 2025 / Accepted: 30 March 2026
Published online: 14 April 2026

References

1. Damania B, Kenney SC, Raab-Traub N. Epstein-Barr virus: Biology and clinical disease. Cell. 2022;185:3652–70. https://doi.org/10.1016/j.cell.2022.08.026.
2. Dunmire SK, Hogquist KA, Balfour HH. Infectious Mononucleosis. Curr Top Microbiol Immunol. 2015;390:211–40. https://doi.org/10.1007/978-3-319-22822-8_9.
3. Odumade OA, Hogquist KA, Balfour HH. Jr. Progress and problems in understanding and managing primary Epstein-Barr virus infections. Clin Microbiol Rev. 2011;24:193–209. https://doi.org/10.1128/cmr.00044-10.
4. Hjalgrim H, Smedby KE, Rostgaard K, Molin D, Hamilton-Dutoit S, Chang ET, et al. Infectious mononucleosis, childhood social environment, and risk of Hodgkin lymphoma. Cancer Res. 2007;67:2382–8. https://doi.org/10.1158/0008-5472.Can-06-3566.
5. Xu Y, Hiyoshi A, Smith KA, Piehl F, Olsson T, Fall K, et al. Association of Infectious Mononucleosis in Childhood and Adolescence With Risk for a Subsequent Multiple Sclerosis Diagnosis Among Siblings. JAMA Netw Open. 2021;4:e2124932. https://doi.org/10.1001/jamanetworkopen.2021.24932.
6. Womack J, Jimenez M. Common questions about infectious mononucleosis. Am Fam Physician. 2015;91:372–6.
7. Wu B, Guo J, Wang J, Feng J, Xu J. Adipose-derived stem cell extracellular vesicles attenuate liver fibrosis via restoration of gut barrier function and

modulation of gut microbiota. Extracell Vesicles Circ Nucl Acids. 2025;6:843–59. https://doi.org/10.20517/evcna.2025.95.
8. Kalluri R, LeBleu VS. The biology, function, and biomedical applications of exosomes. Science. 2020;367. https://doi.org/10.1126/science.aau6977.
9. Yang L, Li J, Li S, Dang W, Xin S, Long S, et al. Extracellular Vesicles Regulated by Viruses and Antiviral Strategies. Front Cell Dev Biol. 2021;9:722020. https://doi.org/10.3389/fcell.2021.722020.
10. Bernea EG, Suica VI, Uyy E, Cerveanu-Hogas A, Boteanu RM, Ivan L, et al. Exosome Proteomics Reveals the Deregulation of Coagulation, Complement and Lipid Metabolism Proteins in Gestational Diabetes Mellitus. Molecules. 2022;27:5502. https://doi.org/10.3390/molecules27175502.
11. Tan Y, Kao WC, Boppart M, Sweedler JV. Plasma-Derived Extracellular Vesicle Proteomics. J Proteome Res. 2025;24:4309–21. https://doi.org/10.1021/acs.jproteome.5c00316.
12. Cao P, Zhang M, Wang W, Dai Y, Sai B, Sun J, et al. Fluorescence in situ hybridization is superior for monitoring Epstein Barr viral load in infectious mononucleosis patients. BMC Infect Dis. 2017;17:323. https://doi.org/10.1186/s12879-017-2412-y.
13. Ma J, Chen T, Wu S, Yang C, Bai M, Shu K, et al. iProX: an integrated proteome resource. Nucleic Acids Res. 2019;47:D1211–7. https://doi.org/10.1093/nar/gky869.
14. Zweig MH, Campbell G. Receiver-operating characteristic (ROC) plots: a fundamental evaluation tool in clinical medicine. Clin Chem. 1993;39:561–77.
15. Perkins NJ, Schisterman EF. The inconsistency of optimal cutpoints obtained using two criteria based on the receiver operating characteristic curve. Am J Epidemiol. 2006;163:670–5. https://doi.org/10.1093/aje/kwj063.
16. Haruta K, Suzuki T, Yamaguchi M, Fukuda Y, Torii Y, Takahashi Y, et al. Comparison of plasma proteomic profiles of patients with Epstein-Barr virus-associated hemophagocytic lymphohistiocytosis and infectious mononucleosis. J Med Virol. 2024;96:e29450. https://doi.org/10.1002/jmv.29450.
17. Chen B, Chen Y, He Z, Pan Y, Luo Y, Yan J, et al. S146 and M148 within the mature chain domain of PSMB4 are crucial for degrading PRRSV nsp1α. Cell Mol Life Sci. 2025;82:148. https://doi.org/10.1007/s00018-025-05679-9.
18. Wang Y, Tong W, Qin W, Yang X, Yu H, Zheng H, et al. Midnolin inhibits coronavirus proliferation by degrading viral proteins. J Virol. 2025;99:e0036625. https://doi.org/10.1128/jvi.00366-25.
19. Kim J, Zhao Y, Kim HY, Kim S, Jiang Y, Lee MJ. Extracellular Vesicle-Mediated Delivery of 20S Proteasomes Enhances Tau Degradation in Recipient Cells. J Extracell Vesicles. 2025;14:e70086. https://doi.org/10.1002/jev2.70086.
20. Sánchez-López CM, Soler C, Garzo E, Fereres A, Pérez-Bermúdez P, Marcilla A. Phloem sap from melon plants contains extracellular vesicles that carry active proteasomes which increase in response to aphid infestation. J Extracell Vesicles. 2024;13:e12517. https://doi.org/10.1002/jev2.12517.
21. Jin M. Unique roles of tryptophanyl-tRNA synthetase in immune control and its therapeutic implications. Exp Mol Med. 2019;51:1–10. https://doi.org/10.1038/s12276-018-0196-9.
22. Lee HC, Lee ES, Uddin MB, Kim TH, Kim JH, Chathuranga K, et al. Released tryptophanyl-tRNA synthetase stimulates innate immune responses against viral infection. J Virol. 2019;93. https://doi.org/10.1128/jvi.01291-18.
23. Qin R, Zhao C, Wang CJ, Xu W, Zhao JY, Lin Y, et al. Tryptophan potentiates CD8(+) T cells against cancer cells by TRIP12 tryptophanylation and surface PD-1 downregulation. J Immunother Cancer. 2021;9. https://doi.org/10.1136/jitc-2021-002840.
24. Aslan N, Watkin LB, Gil A, Mishra R, Clark FG, Welsh RM, et al. Severity of acute infectious mononucleosis correlates with cross-reactive influenza CD8 T-cell receptor repertoires. mBio. 2017;8. https://doi.org/10.1128/mBio.01841-17.
25. Wang Y, Luo Y, Tang G, Ouyang R, Zhang M, Jiang Y, et al. HLA-DR Expression Level in CD8(+) T Cells Correlates With the Severity of Children With Acute Infectious Mononucleosis. Front Immunol. 2021;12:753290. https://doi.org/10.3389/fimmu.2021.753290.
26. Najimi N, Zahednasab H, Farahmand M, Fouladvand A, Talei GR, Bouzari B, et al. Exploring the role of tryptophanyl-tRNA synthetase and associations with inflammatory markers and clinical outcomes in COVID-19 patients: A case-control study. Microb Pathog. 2023;183:106300. https://doi.org/10.1016/j.micpath.2023.106300.
27. Kim KS, Suh GJ, Jin M, Kwon WY, Jung YS, Kim T, et al. Secreted tryptophanyl-tRNA synthetase 1 is a prognostic marker in sepsis patients without monocytopenia. Shock. 2024;61:55–60. https://doi.org/10.1097/shk.0000000000002259.
28. Kim YT, Huh JW, Choi YH, Yoon HK, Nguyen TT, Chun E, et al. Highly secreted tryptophanyl tRNA synthetase 1 as a potential theranostic target for hypercytokinemic severe sepsis. EMBO Mol Med. 2024;16:40–63. https://doi.org/10.1038/s44321-023-00004-y.
29. McCarthy MK, Weinberg JB. The immunoproteasome and viral infection: a complex regulator of inflammation. Front Microbiol. 2015;6:21. https://doi.org/10.3389/fmicb.2015.00021.
30. Goetzke CC, Althof N, Neumaier HL, Heuser A, Kaya Z, Kespohl M, et al. Mitigated viral myocarditis in A/J mice by the immunoproteasome inhibitor ONX 0914 depends on inhibition of systemic inflammatory responses in CoxsackievirusB3 infection. Basic Res Cardiol. 2021;116:7. https://doi.org/10.1007/s00395-021-00848-w.
31. Cheng S, Duan D, Cui H, Lian Y, Jiang F, Chen Q, et al. Serum amyloid A: multifaceted roles in inflammation and cellular interactions. Immunol Res. 2025;73:148. https://doi.org/10.1007/s12026-025-09704-8.
32. Marta-Enguita J, Navarro-Oviedo M, Rubio-Baines I, Aymerich N, Herrera M, Zandio B, et al. Association of calprotectin with other inflammatory parameters in the prediction of mortality for ischemic stroke. J Neuroinflammation. 2021;18:3. https://doi.org/10.1186/s12974-020-02047-1.
33. Zollinger AJ, Smith ML. Fibronectin, the extracellular glue. Matrix Biol. 2017;60–61:27–37. https://doi.org/10.1016/j.matbio.2016.07.011.
34. Efthymiou G, Saint A, Ruff M, Rekad Z, Ciais D, Van Obberghen-Schilling E. Shaping Up the Tumor Microenvironment With Cellular Fibronectin. Front Oncol. 2020;10:641. https://doi.org/10.3389/fonc.2020.00641.
35. Sepulveda JL, Wu C. The parvins. Cell Mol Life Sci. 2006;63:25–35. https://doi.org/10.1007/s00018-005-5355-1.
36. Torres-Durán M, Lopez-Campos JL, Barrecheguren M, Miravitlles M, Martinez-Delgado B, Castillo S, et al. Alpha-1 antitrypsin deficiency: outstanding questions and future directions. Orphanet J Rare Dis. 2018;13:114. https://doi.org/10.1186/s13023-018-0856-9.

Publisher's note